Tuning Selectivities in Gas Separation Membranes Based on Polymer-Grafted Nanoparticles

Tuning Selectivities in Gas Separation Membranes Based on Polymer-Grafted Nanoparticles

Connor R. Bilchak,[1] Mayank Jhalaria,[1] Yucheng Huang,[2] Zaid Abbas,[2,3] Jiarul Midya,[4] Francesco M. Benedetti,[5] Daniele Parisi,[6] Werner Egger,[7] Marcel Dickmann,[7] Matteo Minelli,[8] Ferruccio Doghieri,[8] Arash Nikoubashman,[4] Christopher J Durning,[1] Dimitris Vlassopoulos,[6] Jacques Jestin,[9] Zachary P. Smith[5] Brian C. Benicewicz,[2] Michael Rubinstein,[10] Ludwik Leibler,[11] Sanat K. Kumar[1*]

[1] Department of Chemical Engineering, Columbia University, New York, NY, USA.
[2] Department of Chemistry and Biochemistry, University of South Carolina, Columbia, SC, USA.
[3] Department of Chemistry, Wasit University, Hay Al-Rabea, Kut, Wasit, Iraq 52001.
[4] Institute of Physics, Johannes Gutenberg University Mainz, Staudingerweg 7, D-55128 Mainz, Germany.
[5] Department of Chemical Engineering, Massachusetts Institute of Technology, Cambridge, MA 02139, USA.
[6] University of Crete, Department of Materials Science and Technology, and FORTH, Institute of Electronic Structure and Laser, Heraklion, Greece.
[7] Universität der Bundeswehr München, Institut für Angewandte Physik und Messtechnik LRT2, Werner-Heisenberg-Weg 39, Neubiberg D-85577, Germany.
[8] Department of Chemical Engineering, University of Bologna, Bologna, Italy.
[9] Laboratoire Léon Brillouin (LLB), CEA/CNRS UMR 12, CEA Saclay, 91191, Gif/Yvette Cedex France.
[10] Department of Mechanical Engineering and Materials Science, Biomedical Engineering, Chemistry and Physics, Duke University, Durham, NC, USA.
[11] Laboratoire Gulliver, CNRS UMR 7083, ESPCI Paris, PSL Research University, 75005 Paris, France.

Abstract

Polymer membranes are critical to many sustainability applications that require the size-based separation of gas mixtures. Despite their ubiquity, there is a continuing need to selectively affect the transport of different mixture components while enhancing mechanical and aging behavior. Polymer-grafted nanoparticles (GNPs) are a novel platform which dramatically addresses these issues even for 100 nm thick films. Neat GNP materials have higher gas permeability and lower selectivity because they have increased mean free volume relative to the neat polymer. Going beyond this ability to manipulate the mean free volume, the conceptual advance of the present work is our finding that GNPs are spatially heterogeneous transport media, with the addition of the free polymer being able to manipulate this free volume distribution. We show that adding a small amount of appropriately chosen free polymer can dramatically increase the membrane gas selectivity while only moderately reducing small gas permeability, thus leading to membranes with highly enhanced gas separation ability. In particular, added short free chains, which are homogeneously distributed in the polymer layer of the GNP, only reduce the permeability of all gases with no dramatic increases in selectivity. On the other hand, long free chains, which populate the pockets between GNPs, modify the brush structure so that the transport of large solutes are preferentially hindered, leading to large selectivity increases. Thus, the major practical consequence of this work is our ability to favorably manipulate the selective gas transport properties of GNP membranes through the entropic effects associated with the addition of free chains.

Glassy polymeric membranes are routinely used to separate gas mixtures, e.g., for shale gas remediation and carbon capture. Membrane separations are cost-efficient relative to competing technologies but are limited by the tradeoff between gas permeability ($P_i = D_i \times S_i$, P_i is proportional to throughput, D_i is the gas diffusivity and S_i its solubility coefficient) and selectivity. The ideal selectivity, $\alpha_{ij} = P_i/P_j$, is frequently used as a proxy for product purity. The compromise between P_i and α_{ij} is captured by empirical Robeson upper bound correlations, e.g., shown in Figure 1A, which define the best available polymers for a given separation, in this case of CO_2

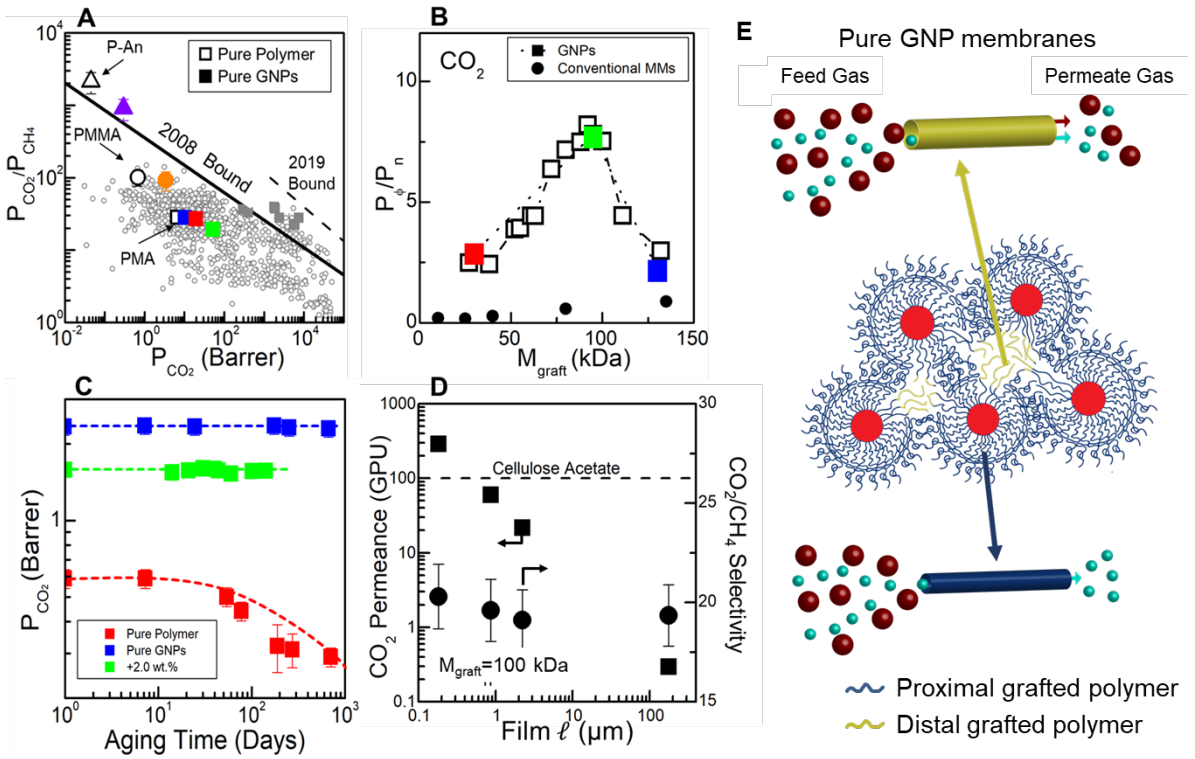

Figure 1: Gas transport in neat GNPs. (A) Robeson plot for CO_2/CH_4 separations (1 Barrer = 1×10^{-10} cm^3(STP)cm/cm^2 s cmHg); solid line: 2008 upper bound.[9] Dashed line: 2019 upper bound.[14] Small open grey symbols are literature data on neat polymers; small filled grey squares are TR polymers. Data for neat PMA, PMMA and Polyaniline (P-An)-based (□, ○, and △ respectively) membranes are in black; data for the neat GNP membranes at constant grafting density σ [≈ 0.5 chains/nm^2 for PMA (filled squares) and PMMA (filled circle); 0.25 chains/nm^2 for PAn-based (filled triangle)] are in color. The three points for the PMA are for different graft molecular weights (M_{graft} ≈ 30 (red), 100 (green) and 130 kDa (blue)). (B) Plot of the ratio of CO_2 permeability in the PMA GNPs (P_ϕ) to that in the neat polymer (P_n) as a function of M_{graft} for σ ≈ 0.5 chains/nm^2. Open symbols are from Ref. 24; colored squares are PMA data in (A). The black circles are corresponding MMMs with NP loadings commensurate with the GNP data. (C) Aging behavior of ℓ ≈ 700 nm thick samples of PMMA GNPs (M_{graft} ≈ 100 kDa, σ ≈ 0.5 chains/nm^2) compared to neat PMMA and blends of the GNPs and neat polymer (2 wt%, 90 kDa). Lines are guides to the eye. The corresponding PMA-based materials show no aging behavior. (D) CO_2 permeance (■) and CO_2/CH_4 selectivity (●) of the most permeable PMA GNPs as a function of film thickness. The dashed line is the permeance of cellulose acetate (100 GPU), a common industrial benchmark. Films as thin as ℓ ≈ 100nm are readily produced via spin-casting. (E) Schematic of neat GNP membranes. The grafted chains must extend to fill in space between the GNP, which constitute the distal regions in the membranes.

from CH_4.[1-3] Many past approaches for improving polymer membrane performance have focused on the synthesis of new materials e.g., polyanilines,[4] thermally rearranged (TR) polymers,[5] and polymers of intrinsic microporosity (PIMs),[6] which contain rigid backbones that frustrate local polymer chain packing. The development of these novel materials has favorably shifted performance, e.g., from the 2008 to the 2019 upper bound.[7] While these materials are empirically found to improve performance, the ability to *a priori* design materials with enhanced permeability/selectivity, improved strength and aging behavior, remains an open challenge.

A potential means to rationally improve performance is to add nanoparticles (NPs), e.g., fumed silica or metal-organic frameworks, to the polymer to form "mixed-matrix" membranes (MMM).[8-12] Previous work has shown that, while these composite materials sometimes improve gas transport, they are frequently accompanied by challenges, including NP aggregation caused by the immiscibility between the inorganic NPs and the organic polymer.[8, 10, 11, 13, 14] The addition of NPs can, however, mitigate aging and plasticization behavior, and improve some mechanical properties of the polymer, all highly desirable traits.[15, 16]

A resolution to the miscibility problem associated with adding (polar) NPs into an apolar polymer, which ensures good NP dispersion, is to chemically graft the polymers to the NP to create GNPs (Figure 1E) with no free chains.[17-20] We have previously shown that neat GNPs have higher gas permeability and lower selectivity relative to the neat polymer (with no added NPs), evidently because they have increased <u>mean</u> free volume. The grafted polymer chains, especially in the limit of dense grafting ("brush" regime), must stretch out to fill all empty space between the NPs (incompressibility constraint). This chain extension evidently results in the increased free volume. The conceptual advance of the present work is our finding that GNPs are spatially heterogeneous transport media, i.e., there are distinct spatial regions with different free volume. We can thus

manipulate the underlying free volume distribution, and hence gas selectivity, with the addition of an appropriately chosen free polymer. This selectivity increase is sensitive to the amount and molecular weight of the free polymer chain added, and maximum selectivity enhancement is found when the graft and free polymer chain lengths are roughly equal to each other. Mechanistically, these long chains populate the distal pockets between the GNPs (and also reduce chain extension), and evidently allow us to selectively manipulate the higher end tail of this distribution. Shorter free chains, which disperse more homogenously in the medium, reduce the chain extension encountered in the pure GNP, but do not selectively block the distal spaces. These shorter added free chains thus do not yield such selectivity increases. We thus speculate that the larger free volume pockets, which selectively help in the transport of large gases, likely must be located in the distal (interstital) regions between the NPs (Figure 1E).

Results and Discussion

Systems Considered and Methods Used: We primarily studied GNPs composed of impermeable silica NPs of diameter 14$\pm$4 nm grafted with poly(methyl acrylate) [PMA] at a grafting density $\sigma \approx$ 0.5 chains/nm^2 ($\approx$ 300 graft chains per NP); the grafted polymer molecular weight, M_{graft}, is systematically varied.[20] Even thin (ℓ = 100nm) GNP films remain easily processable and the NPs serve to increase the shear modulus of the polymer (see Supporting Information, Sample Preparation & Transport Performance Measurements).[15] -We previously considered non-equilibrium pure gas transport of these PMA GNPs measured using the quartz crystal microbalance with dissipation (QCM-D) method, which provides direct measurements of both S_i and D_i. These are directly related to P_i in the framework of the solution-diffusion model, i.e., $P_i = D_i \times S_i$. Here, we complement these data with steady-state light gas permeabilities measured using the constant-volume, variable-pressure method on supported films with $\ell \geq$ 100 nm and thicker free-standing films (see Supporting Information, Materials and Methods). We note that

these two experimental methods have different ranges of validity - the steady-state method with free standing films with ℓ = 30 μm can measure 10^3 Barrer > P_i > 0.07 Barrer, while for the thinnest supported film with ℓ = 100 nm the lower limit is 2×10^{-4} Barrer. QCM-D, a variant of the classical sorption method, is restricted to 80 Barrer > P_i > 5×10^{-6} Barrer. We cross-validate the methods against each other where possible, and use the most appropriate method in each context. Mixed-gas P_i was also measured for the CO_2/CH_4 gas pair by systematically changing composition and pressure and by coupling a specially designed permeation system to an in-line gas chromatograph.

<u>Summary of Pure Gas Permeability Results:</u> Figure 1B shows the CO_2 permeability enhancement in PMA-based GNPs relative to neat PMA as a function of M_{graft}. The pure gas P_i data agree with literature values for the neat polymer (with no NPs)[21] and neat GNPs.[20] The large CO_2 permeability enhancements in neat GNPs relative to the neat PMA are accompanied by modest decreases in ideal α_{CO_2/CH_4} (i.e., the CH_4 permeability enhancement is larger than that of CO_2), shown as colored squares in Figure 1A; similar results are seen for other gas pairs (see Supporting Information, Additional Figures). The GNP results are unexpected since physical mixtures of PMA and bare silica NPs (i.e., conventional MMMs) at similar loadings yield lower P_i than the neat polymer (Figure 1B, see Supporting Information, Transport Performance Experiments).[8, 13, 14] Similar trends are also found for glassy poly(methyl methacrylate) [PMMA] GNPs over similar ranges of M_{graft} and σ, emphasizing the importance of chain grafting in achieving the P_i enhancements. While the specific chemistry of the chains themselves yield different gas permeability values, the increase in relative permeability on grafting is apparently independent of these chemical details. In a related matter, PMMA GNPs in both supported and free-standing film configurations show no deleterious aging effects often encountered in polymer membranes[22, 23] even though the PMMA is glassy under experimental conditions (35°C ,$T_g \approx$ 105

°C, Figure 1C); PMA GNPs (PMA $T_g \approx 18°C$), which are rubbery at 35°C, expectedly show no aging.[20] Further, the permeance (i.e., P/ℓ) of PMA GNPs with $\ell \leq 700$ nm rivals that of commercial cellulose acetate membranes (Figure 1D), an important industrial benchmark.

We now focus on understanding the increased P_i of the PMA GNPs relative to the corresponding neat PMA and traditional MMMs (Figure 1B). Since gas solubilities are found to be hardly affected by grafting,[20] the P_i increases primarily reflect increases in diffusion, likely due to increased "free volume" in the GNPs relative to the MMM (i.e., the "extra" unoccupied volume in a material that aids solvent diffusion).[20] In agreement with this notion, we found an increased dynamic mean free volume via Positron Annihilation Lifetime Spectroscopy (PALS) measurements; this metric shows a maximum in the vicinity of $M_{graft} \approx 80$ kDa. Similarly, density measurements via pycnometry showed that increasing M_{graft} up to ≈ 80 kDa results in progressively larger equilibrium molar volumes than that expected from a linear combination of the NP and polymer.[20] This finding is supported by molecular dynamics (MD) simulations which show lower polymer densities in these GNPs (See Supporting Information, Simulations). Linear rheology experiments show that GNPs display colloidal glass behavior for $M_{graft} < 80$kDa, consistent with a jammed solid state, whereas GNPs with larger M_{graft} behave akin to star polymer melts (See Supporting Information, Rheology). Increases in free volume and hence P_i are therefore correlated with the formation of a jammed solid state.[24]

In the jammed state, the polymer chains must stretch out to fill all empty space between the NPs (incompressibility constraint, Figure 1E). For long enough chains and high enough grafting densities, the brush is comprised of two spatial regions – an inner extended brush and an outer brush following Gaussian statistics where chains from neighboring NPs can interpenetrate.[25] The degree of extension in the inner region depends on the graft chain length, and the highest free volume state (and hence highest gas P_i) corresponds to the brushes with the most extended

chains. Based on a newly published theory, we conjecture that this state of maximum chain extension is in the vicinity of M_{graft} ~ 80kDa. For shorter M_{graft}, chain extension is lower, resulting in lower GNP free volume (but still larger than in the neat polymer) and smaller P_i enhancements. Similarly, for M_{graft} larger than 80kDa, in the star-polymer regime, the interpenetration region becomes dominant and hence the permeability decreases with increasing M_{graft}, till it is eventually akin to that of the neat polymer.[24, 26]

Role of Added Polymer: Figure 1A further suggests that the permeability vs. ideal selectivity data for the neat PMA (black open squares) and the PMA-based GNPs (colored squares), when considered together, run almost parallel to the Robeson upper bound. These data are thus consistent with Cohen and Turnbull's[27] model of a single, mean free volume metric controlling transport and thus the permeability/selectivity tradeoff: $\log \alpha_{A/B} \sim \left(1 - \frac{v_B}{v_A}\right) \log P_A + c$, where v_A and v_B are related to the sizes of the gas molecules (in this framework, $v_B > v_A$). GNPs in the jammed state have higher free volume rationalizing the increased P_i on grafting and the peak permeability in Figure 1B.[20] Since the free volume in these jammed states is higher than in the pure melt (with no NPs), we conjecture that the addition of solutes, in particular free polymer chains of molecular weight M_{free}, can help to manipulate this quantity. This methodology could thus provide us with a simple way to controllably vary gas permeability in these constructs. We then expect both CO_2 and CH_4 permeabilities to decrease with increasing ω_{free}, the free polymer loading (in wt.%), and CO_2/CH_4 selectivity to increase monotonically (i.e., follow a line with a negative slope parallel to the upper bound correlation in Figure 1A).

To verify this conjecture, we considered both PMA and PMMA-based GNP membranes with the highest permeability, i.e., the state with the largest chain extension (M_{graft} ≈ 100 kDa at $\sigma \approx 0.5$

chains/nm^2; other M_{graft} and σ data are in the Supporting Information, Additional Figures). These GNPs were mixed with chemically identical polymers of various M_{free} at different ω_{free}. Each sample was mixed in solution, followed by drying in an ambient atmosphere and thermal annealing above the polymer glass transition temperature for 2 days. Electron microscopy and X-Ray Scattering (see Supporting Information, X-Ray/Neutron Scattering) show that free chains and GNPs of the same polymer chemistry are miscible for all M_{free} considered.[28] In the gas transport

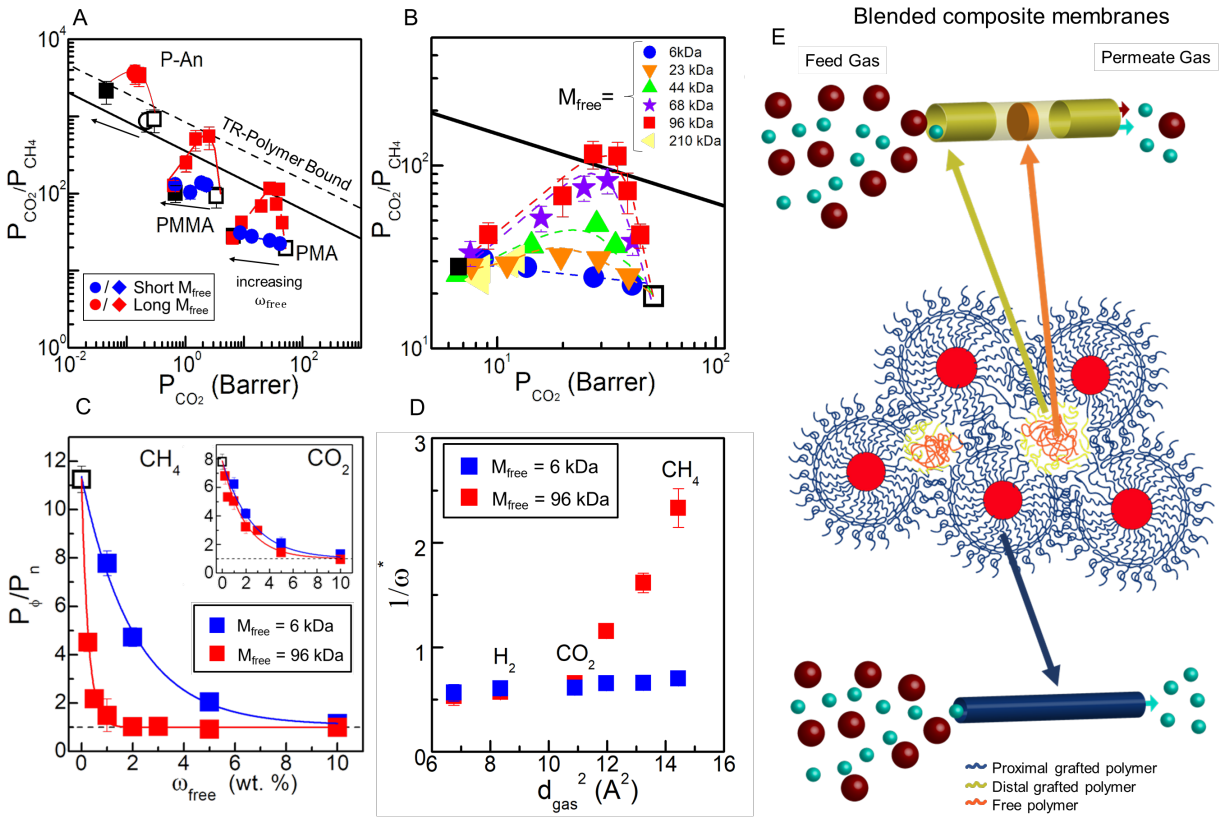

Figure 2: Pure gas transport in GNP/free chain mixtures. (A) CO_2/CH_4 Robeson plot of PMA-grafted and PMMA-grafted NP membranes at similar conditions (for PMA $M_{graft} \approx 100$ kDa, $M_{free} \approx 6$ kDa "short" free chains, and $M_{free} \approx 96$ kDa "long" chains; for PMMA, $M_{graft} \approx 100$ kDa, $M_{free} \approx 3$ kDa "short" free chains, and $M_{free} \approx 90$ kDa "long" chains) and PAn-based composites ($M_{graft} \approx 30$ kDa; $M_{free} \approx 30$ kDa). The solid black line is the 2008 Robeson upper bound.[9] (B) CO_2/CH_4 selectivity enhancements for PMA GNPs ($M_{graft} \approx 100$ kDa) with different M_{free} and weight fractions. The neat PMA GNP is the open black square symbol and the weight fractions of the free chains increase for all mixtures on moving from right to left. Maximum selectivity enhancements are observed for $M_{free} \approx 96$ kDa. (C) CH_4 permeability enhancement in PMA-grafted GNP composites with added $M_{free} \approx 6$ kDa and $M_{free} \approx 96$ kDa, respectively, at various ω_{free}; Inset: permeability enhancement of CO_2. (Data for other M_{free} and gases are in the Supporting Information, Additional Figures). The solid lines are fits to $\frac{P_\phi}{P_n} = 1 + \beta_{\phi,0} e^{-\omega_{free}/\omega^*}$. (D) ω^* plotted a function of the gas kinetic diameter d_{gas}^2 in PMA based composites with two different M_{free}. $\beta_{\phi,0}$ is reported in the Supporting Information. (E) Schematic of gas transport in the blended composite systems. Added free chains with large M_{free} preferentially segregate into the distal regions and reduce the transport of larger gases; the whole grafted polymer transports the smaller molecules.

measurements of blends with low molecular weight free chains (PMA, $M_{free} \approx$ 6 kDa mixed with PMA GNPs; PMMA, $M_{free} \approx$ 3 kDa mixed with PMMA GNPs) we found that increasing ω_{free} leads to a monotonically decreasing P_{CO_2} and slightly increasing α_{CO_2/CH_4} (Figure 2A). Since the transport of both species is affected similarly by the addition of free chains, we emphasize the notion that both gases experience the same mean free volume, which is decreased by increasing the ω_{free} of a low M_{free} additive. These trends are expected, as discussed above.

In contrast, blends with long free chains ($M_{free} \approx$ 96 kDa), comparable in length to the brush, demonstrate unexpected, non-monotonic permeability/selectivity behavior with increasing ω_{free}. Figure 2A shows large (≈ 6x) increases in CO_2/CH_4 selectivity for the PMA based system with $\omega_{free} \approx$ 1 - 2 wt.%. Blends with ω_{free} > 10 wt.% have transport properties comparable to that of the neat polymer. The ideal selectivities of PMA-based blends approach the 2008 Robeson upper bound (within experimental error), while the corresponding best-performing PMMA materials exceed this empirical limit and perform comparably to TR polymers (see Figure 2A).

This behavior is not unique to this PMA M_{free}. We find that progressively smaller M_{free} yield progressively smaller selectivity increases at each loading when compared to $M_{free} \approx$ 96 kDa (Figure 2B). Similarly, increasing M_{free} beyond 96 kDa (up to 210 kDa) also results in a monotonic decrease in selectivity. The condition where $M_{free} \approx M_{graft}$ evidently corresponds to the optimal conditions for maximizing ideal selectivity, while at the same time still yielding improved permeabilities relative to the neat PMA. Experiments on analogous blended Poly(aniline) [Pan] systems with $M_{graft} \approx M_{free} \approx$ 30 kDa, $\sigma \approx$ 0.25 chains/nm^2 exceed even the upper bound defined by TR polymers, and display extraordinarily high selectivities and no measurable loss of performance over time (Figure 2A, measured using QCM-D; see Supporting Information, Additional Figures). These results are also observed for other gas pairs, though its degree

correlates directly with the ratio of the kinetic diameters of the gases, d_A/d_B. Pairs with smaller, but similar d_{gas} values (e.g., He/H_2, Supporting Information, Additional Figures) fall well below the upper bound and perform similarly to what was found in the case of the neat PMA, regardless of M_{free}; other pairs with disparate d_{gas} (e.g., H_2/CH_4, Supporting Information, Additional Figures) well exceed their upper bounds. Evidently, while using neat GNPs primarily increases gas permeability and moderately reduces selectivity, adding small amounts of appropriately chosen free polymer dramatically increases gas selectivity while only moderately reducing small gas P_i, allowing us to achieve unprecedented performance improvements that are readily tunable through polymer chemistry and M_{free}.

To gain a more detailed understanding of these central results, Figure 2C and its inset compare the gas permeability enhancements of PMA-based blended materials for both short and long M_{free}. Each set of data is well-fit by the empirical equation: $\frac{P_\phi}{P_n} = 1 + \beta_{\phi,0} e^{-\omega_{free}/\omega^*}$,[8] where ω^* is the sensitivity of permeability enhancement to the added homopolymer. For systems described by a single effective free volume, ω^* should be independent of the kinetic diameter of the gas, d_{gas}. Indeed, for $M_{free} \approx 6$ kDa, $\omega^* \approx 2$ wt.% and only weakly dependent on d_{gas} (Figure 2D). As expected, this indicates that the free chains simply serve to reduce the mean free volume, and that the permeability of differently sized gases are affected in a similar manner with ω_{free} variations. The $M_{free} \approx 96$ kDa data, in contrast, show that gases with $d_{gas} < 0.35$ nm have $\omega^* \approx$ 2 wt.% comparable to the $M_{free} \approx 6$ kDa composites, while larger gas molecules have smaller ω^* (Figure 2D); for example, for CH_4, $\omega^* \approx$ 0.4 wt.%. Said differently, while the P_i of the smaller CO_2 molecules (d_{gas} = 0.33 nm) are effectively independent of M_{free}, the larger CH_4 molecules (d_{gas} = 0.38 nm) are very sensitive to M_{free}. The low M_{free} data for CH_4 (Figure 2C, blue points) follow the CO_2 trends but the high M_{free} data (red points) show a much stronger dependence. Thus,

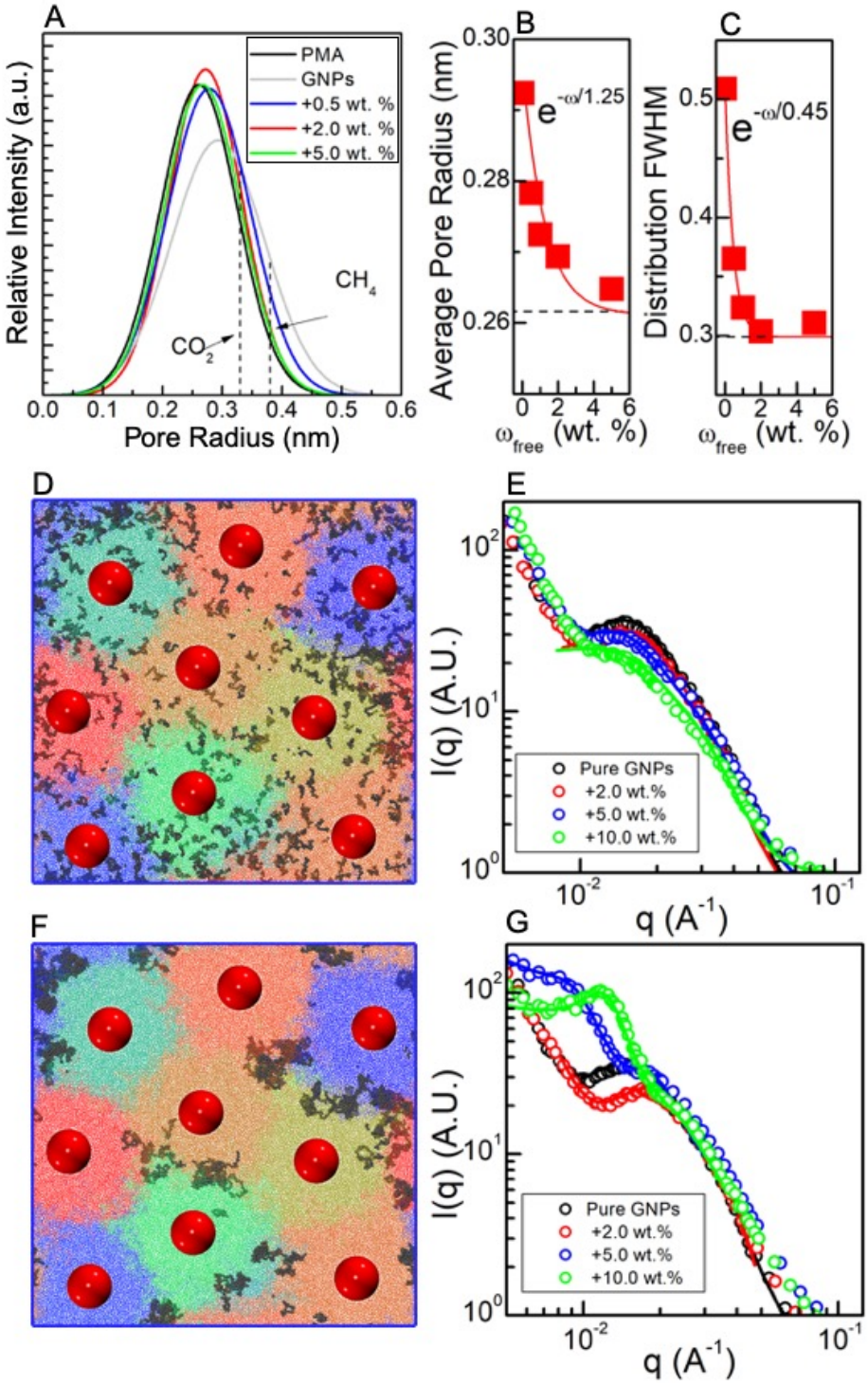

Figure 3: (A) PALS determined free volume distributions in PMA GNPs ($\sigma \approx 0.5$ chains/nm^2, $M_{graft} \approx 100$ kDa) and composites with added $M_{free} \approx 96$ kDa. (B,C) Moments of ortho-positronium (o-Ps) lifetime distributions in the composites. (B) Average radius and (C) the full-width at half-maximum (FWHM, related to the distribution of radii). (D,F) Molecular Dynamics simulations of GNPs with $M_{graft} \approx 75$ kDa, $\sigma = 0.47$ chains/nm^2 containing 2 wt.% added free chains of length (D) $M_{free} \approx 5$ kDa, and (F) $M_{free} \approx 75$ kDa. Each NP, shown in red, has a diameter of 15 nm. Free polymers are shown in grey; each NP's polymer corona is colored differently for distinction. (E) and (G) Small Angle Neutron Scattering (SANS) profiles of PMMA-grafted NPs ($M_{graft} \approx 100$ kDa. $\sigma \approx 0.5$ chains/nm^2) with added deuterated PMMA free chains with (E) $M_{free} \approx 3$ kDa and (G) $M_{free} \approx 90$ kDa. The solid lines are model fits.

selectivity enhancements shown in Figure 2A.

The fact that the selectivity of these high M_{free} blended materials does not track linearly with permeability on a Robeson plot implies that the effective free volume experienced by the two gases are different. This key new conclusion is not apparent in neat GNPs, or in GNPs blended with shorter $M_{free} \approx 6$ kDa homopolymers, and is only found for higher M_{free}. To gain insights into this finding we used PALS to determine ortho-positronium (o-Ps) lifetimes in the composites on the addition of $M_{free} \approx 96$ kDa PMA, which are then translated into free volume distributions (see Supporting Information, PALS); these data are shown in Figure 3A. Evidently, while the free volume distributions are monomodal in all cases, adding increasing amounts of the $M_{free} \approx 96$ kDa homopolymer systematically reduces the mean value (Figure 3B) and full width at half maximum, FWHM, of this distribution (Figure 3C). The mean free volume radius decreases exponentially with ω_{free} (i.e., $e^{-\omega_{free}/1.25}$) and only returns to its neat homopolymer value for $\omega_{free} \geq 5$ wt.%. This dependence tracks the behavior of the permeability of the smaller CO_2 on the addition of free chains ($\sim e^{-\omega_{free}/2}$). In conjunction with the data in Figures 2C (inset) and 2D, evidently, the CO_2 uses the full GNP polymer layer for transport. In contrast, the FWHM ($\sim e^{-\omega_{free}/0.45}$) returns to its neat value for $\omega_{free} \geq 2$ wt.%. This is consistent with the permeability behavior of the CH_4 on the addition of free chains ($\sim e^{-\omega_{free}/0.4}$). Apparently, the permeability of the larger gas is sensitive to the width of the distribution, presumably the tail of the distribution with larger size free volume elements. Thus, we conclude that the two gases transport differently in the GNPs mixed with higher M_{free} because they sample different parts of the free volume distribution. Most importantly these free volume pockets are evidently in different spatial regions of the grafted polymer layers.

<u>Structural Characterization</u>: To gain a structural understanding of these results, we used coarse

grained MD simulations to probe the spatial distribution of short added free chains (M_{free} ≈ 5 kDa) in a chemically-identical brush with M_{graft} ≈ 75 kDa (for details, see Supporting Information, Simulations). In parallel, small angle X-Ray and neutron scattering (SAXS, SANS) experiments were performed on PMMA-grafted NPs (M_{graft} ≈ 100 kDa at σ ≈ 0.5 chains/nm^2) mixed with short free dPMMA chains (M_{free} ≈ 3 kDa) at different ω_{free}. Figure 3D shows that the short free chains (grey) are more homogeneously distributed in the GNP constructs than the long free chains (Figure 3F). Analogous SAXS experiments show that the GNPs remain miscible for all combinations of ω_{free} and M_{free};[20,29] and the NP spacing increases with ω_{free} (see Supporting Information, X-ray/Neutron Scattering).

SANS is further able to distinguish spatial correlations among the silica core, the protonated graft chains (hPMMA) and deuterated free chains (dPMMA). We find only a single SANS correlation peak in short M_{free} composites (Figure 3E), but with an intensity that decreases with added free polymer. Data fitting shows (see Supporting Information, X-ray/Neutron Scattering), within the sensitivity of these experiments, that the short chains are homogeneously distributed in these GNPs, in agreement with the simulations. This result is consistent with past work which has experimentally found that added small solutes (e.g., ethyl acetate) homogeneously distribute themselves in the GNPs.[30]

The spatial distribution of long deuterated PMMA free chains (M_{free} ≈ 90 kDa) is considered next. While SAXS results are consistent with the M_{free} ≈ 3 kDa sample (see Supporting Information, X-ray/Neutron Scattering) and indicate well-dispersed NP cores, there is a new secondary low-q SANS scattering feature in the ω_{free} = 5 wt.% and 10 wt.% samples, evidently corresponding to free dPMMA chains spaced at distances larger than the mean inter-NP separation (Figure 3G). We conclude that the M_{free} ≈ 90 kDa free chains are not homogeneously distributed, but rather

are localized preferentially in the distal (or interstitial) regions within the GNP constructs. These insights are validated by MD simulations, which show that free chains with $M_{free} \approx 75$ kDa at $\omega_{free} = 2$ wt.% segregate into the distal regions (Figure 3F). Previous work on miscible mixtures of copolymers with homopolymers,[31] and mixtures of GNPs[32] echo these findings.

Overall Physical Mechanism: These findings in combination provide the following physical picture that explains the unusual transport behavior of GNP blended composites. We believe that CO_2 and CH_4 are distributed isotropically in the polymer layer at equilibrium (as found for small solvents[30] and also the low M_{free} chains). The CO_2 transport, which tracks the mean distribution of free volumes, implies that the smaller gas diffuses through the whole polymer brush layer (Figure 2E). The larger CH_4 molecules, on the other hand, must primarily move through the larger dynamic free volume "pockets". The question is where these larger free volume pockets are spatially located. On adding long M_{free} ($\approx$ 96 kDa) chains two things happen: (i) SANS shows that these free chains, which have lower free volume in the melt state relative to the corresponding GNP layer, preferentially segregate into the distal regions of the polymer brush, and (ii) the presence of the free chains reduces the packing frustration encountered by these extended graft chains. The graft chains thus become less extended as has been verified using computer simulations. Both of these mechanisms lead to lower free volume. Here we note that the added short chains, which are more spatially homogeneous, reduce the chain stretching but dont fill the distal spaces. Thus, we conclude that the higher end of the free volume distribution (as probed through PALS) is likely in the distal spaces of these brushes, which are in their state of maximum extension in their pure states. The fact that polymer layers preferentially transport gas molecules through pathways based on their size[33] is known and leveraged in rigid TR polymers[5] and Metal-Organic Framework (MOF) based MMMs,[10, 34, 35] but our ability to selectively manipulate these channels through entropic effects, i.e., by adding carefully chosen homopolymer to the GNP layers, is an important new finding.

The critical d_{gas} where two distinct transport pathways manifest (i.e., beyond the d_{gas} at which ω^* becomes d_{gas} dependent in Figure 2D) can be tuned by varying the NP core size. All of the notable results reported here are for films with NPs of core diameter 14 nm where we find maximum gas selectivities in matched composites, i.e., where $M_{free} \approx M_{graft}$, and when M_{graft} corresponds to the state of maximum chain extension. All other cases yielded lower permeabilities. Inspired by these results, we now consider selectivity changes in composites with different NP size using two representative cases; one where $M_{free} \ll M_{graft}$ and one with $M_{free} \approx M_{graft}$ (termed long M_{free}). In contrast to the data on NPs with the 14nm diameter core, composites with 50 nm silica cores show no changes in selectivity for any gas pair that we have studied ($d_{gas} \leq 0.5$ nm, Figure 4A;

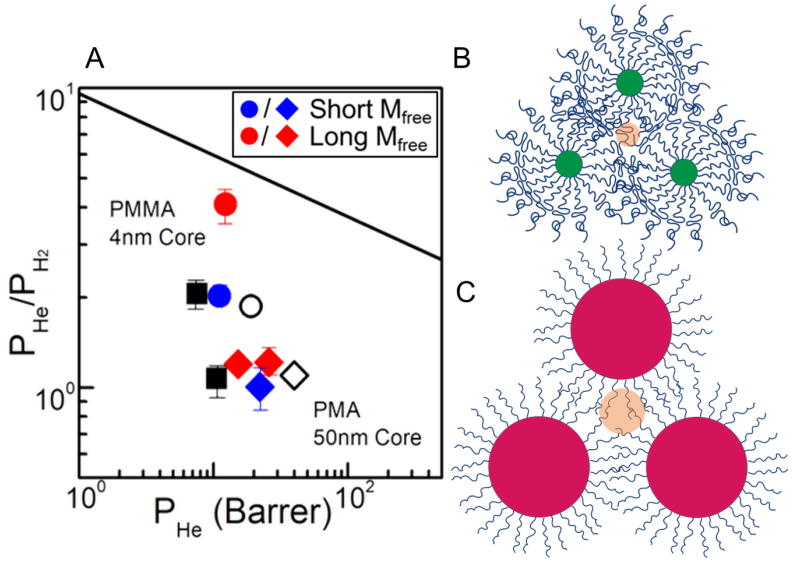

Figure 4: (A) Effect of changing the NP core size on He/H_2 selectivity. Large NPs (50 nm diameter) consistently show effectively no change in selectivity regardless of gas pair, while small NPs (4nm diameter) are able to be designed to selectively separate He and H_2. Filled black symbols are the neat polymers, the open symbols the corresponding neat GNPs and filled symbols mixtures with added free chains. Circles – 4 nm diameter cores ($M_{graft} \approx$ 11 kDa, $\sigma \approx$ 0.25 chains/nm^2), diamonds – 50 nm diameter cores ($M_{graft} \approx$ 100 kDa, $\sigma \approx$ 0.47 chains/nm^2). (B,C) Structural schematic of composites with small (2nm,green) and large(50nm,red) NPs. The small NPs contain substantially smaller distal polymer regions (shown with an orange circle), causing them to be more sensitive to diffusants with smaller d_{gas}; conversely, larger NP materials contain significantly larger sized free volume in the distal regions, reducing the ability of the GNP composites to effectively separate gases based on size.

see Supporting Information, Additional Figures) regardless of M_{free} or ω_{free}. Conversely, while GNPs with 4nm diameter NPs also show no changes in CO_2/CH_4 selectivity, they instead

significantly affect the permeability of smaller gas mixtures, e.g., He/H_2 (Figure 4A). Variations in GNP core size can thus be used to favor the separation of desired gas pairs. Presumably the size of the distal spaces scale with the NP size and provides a simple means of understanding these results. These differences in brush structure, and how they are affected by core size, thus provide a simple handle for manipulating the gas separation efficiency of these constructs.

Preliminary Mixed-Gas Permeability Results: While all of these results have been collected by means of pure gas experiments, industrial applications require the use of non-ideal gas mixtures. Previous work on polymers has shown that CO_2/CH_4 mixed-gas selectivities are typically much lower than those calculated from pure gas permeabilities. This effect is commonly attributed to membrane plasticization by the more soluble gas.[36] To test for this effect in the GNP membranes, we performed preliminary mixed-gas permeation experiments on a representative PMA composite (see Supporting Information, Mixed-Gas Permeability Measurements). In PMA, P_{CO_2} = 6.7 Barrer and its ideal CO_2/CH_4 selectivity α_{ij} = 28. For the PMA GNP sample tested with M_{graft} ≈ 100 kDa, $\sigma \approx 0.5$ chains/nm^2 with added $\omega_{free} \approx 3$ wt.% 96 kDa homopolymer, the pure gas P_{CO_2} = 23 Barrer and its ideal CO_2/CH_4 selectivity α_{ij} = 41$\pm$11. Consistent with this finding, at low pressures (2 bar total pressure, 20% CO_2, 80% CH_4) the mixed-gas permeabilities and selectivities are P_{CO_2} = 21.3 Barrer and α_{ij}= 33$\pm$5; while at high pressures (24 bar total pressure, 50% CO_2, 50% CH_4), the effect of CO_2 plasticization yields P_{CO_2} = 42.6 Barrer and α_{ij}= 23$\pm$3 (see Supporting Information, Mixed-Gas Permeability Measurements).[37] These early results show that the GNP composites demonstrate a 3-6x increase in CO_2 permeability and comparable mixed-gas selectivity for CO_2/CH_4 relative to the ideal behavior of the homopolymer.

Conclusions

In summary, while size-based gas separation is common in polymeric membranes, we have

developed a facile means to selectively control the transport of different mixture components through the addition of free polymer to a GNP based membrane. The significant conceptual advance of this work is the ability to create two spatial regions with different transport properties through the use of GNPs and selectively manipulate them with the tools of polymer physics. This method can greatly improve membrane selectivity and permeability for polymer systems that otherwise show unattractive property sets. In the absence of added homopolymer, or when added small chains are distributed homogeneously, gas transport in the GNPs can be described by a single effective free volume metric.[27] However, if we can selectively block the distal spaces (shown schematically in Figure 2E), the free volume distribution in neat GNPs can be selectively manipulated by a judicious choice of added free polymer. In such situations the transport of the larger gas is affected more dramatically compared to the smaller gas, leading to exceptional membrane selectivities. What constitutes “small” and “large” gases is apparently controlled by the size of the NP cores. The principle underlying this work seems general and should be generally applicable to many classes of polymers and NPs, especially since it synergistically leverages simple chemistries to control localized polymer morphologies. Since film formation relies on simple mixing of the two components, this methodology can be easily integrated into existing membrane production techniques. Our work thus demonstrates that GNP composites represent a novel, easily-realizable platform for next generation gas separation membranes with unprecedented performance metrics.

Methods

Materials and Synthesis: All solvents and materials were used as received. Methyl acrylate (99%, Acros) and methyl methacrylate (99%, Acros) were purified by filtration through an activated basic alumina column. Spherical silica nanoparticles (14 ± 4 nm diameter [MEK-ST] and 53 ± 17 nm diameter [MEK-ST-L]) were obtained from Nissan Chemical. 4 nm diameter ZrO_2 NPs were synthesized using the procedure of Garnweitner *et al*.[38] PMA free chains (matrix) were synthesized by the well-established Reversible Addition-Fragmentation Chain Transfer (RAFT) method[39]. Deuterated PMMA matrices were purchased from Polymer Source and used as received. Grafted NPs were prepared using a Surface-Initiated Reversible Addition-Fragmentation Chain Transfer polymerization (SI-RAFT) synthesis. The RAFT agent 2-(dodecylthiocarbonothioylthio) propanoic acid (DoPAT) used for the polymerization was purchased from Boron Molecular, Inc. Polymer molecular weights and dispersities were determined using gel permeation chromatography calibrated to PMMA standards obtained from Polymer Laboratories. The chemical composition of the chains was determined with ^{1}H NMR and ^{13}C NMR (Bruker Avance 300) using $CDCl_3$ as solvent. Average molecular weights and dispersities of the polymer chains and GNPs are listed in the Supporting Information, Sample Listing.

Gas Transport Experiments: Steady-state gas permeabilities were measured on solution-cast films with thicknesses ranging from ~100 nm up to 120 μm using the constant-volume, variable-pressure technique (typical permeability ranges explored by this method range from ~ 0.07 to $>10^3$ Barrer for 30 μm films, using supported 100 nm thick films shifts the lower bound to ~ 2×10^{-4} Barrer). Thin films were supported with filter paper and mounted onto brass discs of known inner diameter. Gas permeabilities were measured in the following order: H_2, He, O_2, N_2, CH_4, CO_2. Diffusion and solubility coefficients of CO_2 and CH_4 were also determined with QCM-D (Biolin Scientific, Sweden; typical permeability range ~ 5×10^{-6} to 80 Barrer) transient mass uptake experiments on spin-cast films < 5 μm in thickness. AT-cut quartz crystal sensors were cleaned with a 5:1:1 mixture of deionized water, ammonium hydroxide, and hydrogen peroxide and UV-ozone treated before taring the sensor for use as a microbalance. Films were spin-cast from concentrated (> 60 mg/ml) solutions. Gas permeabilities measured with the two techniques agree within experimental error for systems where both methods apply. Error bars represent the standard deviation of at least three independent measurements. Error bars that are not visible are within the size of the symbols. Typical experimental uncertainties are ~5% for materials with permeabilities between 10-80 Barrer, and are ~10% for materials with permeabilities < 0.1 Barrer. Mixed-gas experiments were performed with CO_2/CH_4 mixtures at 35 °C with a constant-volume, variable-pressure permeation system from Maxwell Robotics coupled with an in-line gas chromatograph (Agilent, 7890B). Data were collected at constant pressure (~1.5 bar) and variable composition (ranging from 20 mol.% CO_2 to 50 mol.% CO_2, balance CH_4), as well as constant composition (50 mol.% CO_2, balance CH_4) and variable pressure (up to ~24 bar).

Structural Characterization: SANS was performed on the PA20 spectrometer of the LLB (Saclay, France) at fixed incident wavelength λ = 0.6 nm for 3 sample to detector distances; 1.5, 8 and 19 m. The scattering curves were normalized for sample thickness, transmission, and water scattering to correct for detector heterogeneities. Empty beam and electronic background contributions were subtracted and absolute units were determined as a function of the incident neutron beam intensity. Data reduction was done using the home-made PASINET software and modeling/fitting performed with Sasfit[40]. SAXS experiments were performed on bulk GNP composites using a lab-scale instrument (SAXSlab, Amherst, MA) with a beam cross section 100x100 μm and wavelength λ = 0.154 nm (incident energy of 12.4 KeV) for 4 sample to detector

distances of 1.5, 1.0, 0.5, and 0.05 m, respectively. Samples were ≈ 1 mm in thickness. The data were background subtracted and reported as scattered intensity as a function of momentum transfer, q. The SAXS/USAXS measurements on PMMA composites were done by synchrotron SAXS using the ID02 high-brilliance beamline (ESRF, Grenoble, France), with a beam cross section 200 × 400 μm and wavelength λ = 0.1 nm (incident energy of 12.4 KeV) for 2 sample to detector distances of 1 and 30 m, respectively. SAXS data were recorded on a Rayonix MX-170HS and USAXS on a FReLoN 16M Kodak CCD. The data were treated for angular regrouping and background subtraction, and then reported as intensity as a function of q. Details on the fitting parameters are discussed in the Supporting Information, X-Ray/Neutron Scattering.

PALS experiments were conducted at the pulsed low energy positron system (PLEPS) at the Heinz Maier-Leibnitz Zentrum (Germany) on bulk samples with an implantation energy of 16 keV. The data were analyzed with the PALSFIT3 program.

TEM samples were made by drop casting solutions of 1.00-1.25 mg/ml in 95/5 THF/Chloroform on to Lacey Carbon TEM grids (Electron Microscopy Services, Hatfield, PA) and imaged using a Phillips CM12 TEM.

More information about GNP synthesis, experimental methods and the simulation model can be found in the Supporting Information.

References

1. Robeson, L. M., CORRELATION OF SEPARATION FACTOR VERSUS PERMEABILITY FOR POLYMERIC MEMBRANES. *Journal of Membrane Science* **1991,** *62* (2), 165-185.
2. Robeson, L. M., The upper bound revisited. *Journal of Membrane Science* **2008,** *320* (1-2), 390-400.
3. Sanders, D. E.; Smith, Z. P.; Guo, R. L.; Robeson, L. M.; McGrath, J. E.; Paul, D. R.; Freeman, B. D., Energy-efficient polymeric gas separation membranes for a sustainable future: A review. *Polymer* **2013,** *54* (18), 4729-4761.
4. Hachisuka, H.; Ohara, T.; Ikeda, K.-I.; Matsumoto, K., Gas permeation property of polyaniline films. *J Appl Polym Sci* **1995,** *56* (11), 1479-1485.
5. Park, H. B.; Jung, C. H.; Lee, Y. M.; Hill, A. J.; Pas, S. J.; Mudie, S. T.; Van Wagner, E.; Freeman, B. D.; Cookson, D. J., Polymers with cavities tuned for fast selective transport of small molecules and ions. *Science* **2007,** *318* (5848), 254-258.
6. McKeown, N. B.; Budd, P. M., Polymers of intrinsic microporosity (PIMs): organic materials for membrane separations, heterogeneous catalysis and hydrogen storage. *Chemical Society Reviews* **2006,** *35* (8), 675-683.
7. Comesana-Gandara, B.; Chen, J.; Bezzu, C. G.; Carta, M.; Rose, I.; Ferrari, M. C.; Esposito, E.; Fuoco, A.; Jansen, J. C.; McKeown, N. B., Redefining the Robeson upper bounds for CO2/CH4 and CO2/N-2 separations using a series of ultrapermeable benzotriptycene-based polymers of intrinsic microporosity. *Energy & Environmental Science* **2019,** *12* (9), 2733-2740.
8. Merkel, T. C.; Freeman, B. D.; Spontak, R. J.; He, Z.; Pinnau, I.; Meakin, P.; Hill, A. J., Ultrapermeable, reverse-selective nanocomposite membranes. *Science* **2002,** *296* (5567), 519-522.
9. Koros, W. J.; Zhang, C., Materials for next-generation molecularly selective synthetic membranes. *Nat Mater* **2017,** *16* (3), 289-297.
10. Galizia, M.; Chi, W. S.; Smith, Z. P.; Merkel, T. C.; Baker, R. W.; Freeman, B. D., 50th Anniversary Perspective: Polymers and Mixed Matrix Membranes for Gas and Vapor Separation: A Review and Prospective Opportunities. *Macromolecules* **2017,** *50* (20), 7809-7843.
11. Park, H. B.; Kamcev, J.; Robeson, L. M.; Elimelech, M.; Freeman, B. D., Maximizing the right stuff: The trade-off between membrane permeability and selectivity. *Science* **2017,** *356*.
12. Liu, G.; Chernikova, V.; Liu, Y.; Zhang, K.; Belmabkhout, Y.; Shekhah, O.; Zhang, C.; Yi, S.; Eddaoudi, M.; Koros, W. J., Mixed matrix formulations with MOF molecular sieving for key energy-intensive separations. *Nat Mater* **2018,** *17* (3), 283-289.
13. Takahashi, S.; Paul, D. R., Gas permeation in poly(ether imide) nanocomposite membranes based on surface-treated silica. Part 1: Without chemical coupling to matrix. *Polymer* **2006,** *47* (21), 7519-7534.
14. Lin, H. Q.; Freeman, B. D., Materials selection guidelines for membranes that remove CO2 from gas mixtures. *Journal of Molecular Structure* **2005,** *739* (1-3), 57-74.
15. Priestley, R. D.; Ellison, C. J.; Broadbelt, L. J.; Torkelson, J. M., Structural relaxation of polymer glasses at surfaces, interfaces and in between. *Science* **2005,** *309* (5733), 456-459.
16. Bilchak, C. R.; Huang, Y.; Benicewicz, B. C.; Durning, C. J.; Kumar, S. K., High-Frequency Mechanical Behavior of Pure Polymer-Grafted Nanoparticle Constructs. *ACS Macro Letters* **2019,** *8* (3), 294-298.
17. Akcora, P.; Liu, H.; Kumar, S. K.; Moll, J.; Li, Y.; Benicewicz, B. C.; Schadler, L. S.; Acehin, D.; Panagiotopoulos, A. Z.; Pryamitsyn, V.; Ganesan, V.; Ilavsky, J.; Thiyagarajan, P.; Colby, R. H.; Douglas, J. F., Anisotropic particle self-assembly in polymer nanocomposites. *Nat Mater* **2009,** *8*, 354-359.

18. Kumar, S. K.; Jouault, N.; Benicewicz, B.; Neely, T., Nanocomposites with Polymer Grafted Nanoparticles. *Macromolecules* **2013,** *46* (9), 3199-3214.
19. Ohno, K.; Morinaga, T.; Takeno, S.; Tsujii, Y.; Fukuda, T., Suspensions of silica particles grafted with concentrated polymer brush: A new family of colloidal crystals. *Macromolecules* **2006,** *39* (3), 1245-1249.
20. Bilchak, C. R.; Buenning, E.; Asai, M.; Zhang, K.; Durning, C. J.; Kumar, S. K.; Huang, Y.; Benicewicz, B. C.; Gidley, D. W.; Cheng, S.; Sokolov, A. P.; Minelli, M.; Doghieri, F., Polymer-Grafted Nanoparticle Membranes with Controllable Free Volume. *Macromolecules* **2017,** *50* (18), 7111-7120.
21. Mogri, Z.; Paul, D. R., Gas sorption and transport in poly(alkyl (meth)acrylate)s. I. Permeation properties. *Polymer* **2001,** *42* (18), 7765-7780.
22. Tiwari, R. R.; Jin, J. Y.; Freeman, B. D.; Paul, D. R., Physical aging, CO2 sorption and plasticization in thin films of polymer with intrinsic microporosity (PIM-1). *Journal of Membrane Science* **2017,** *537*, 362-371.
23. Huang, Y.; Wang, X.; Paul, D. R., Physical aging of thin glassy polymer films: Free volume interpretation. *Journal of Membrane Science* **2006,** *277* (1-2), 219-229.
24. Gury, L.; Gauthier, M.; Cloitre, M.; Vlassopoulos, D., Colloidal Jamming in Multiarm Star Polymer Melts. *Macromolecules* **2019,** *52* (12), 4617-4623.
25. Midya, J.; Rubinstein, M.; Kumar, S. K.; Nikoubashman, A., Structure of solvent-free polymer grafted nanoparticles. *Submitted*.
26. Daoud, M.; Cotton, J. P., Star Shaped Polymers - A Model for the Conformation and its Concentration Dependence. *Journal De Physique* **1982,** *43* (3), 531-538.
27. Cohen, M. H.; Turnbull, D., Molecular Transport in Liquids and Glasses. *J Chem Phys* **1959,** *31* (5), 1164-1169.
28. Borukhov, I.; Leibler, L., Enthalpic stabilization of brush-coated particles in a polymer melt. *Macromolecules* **2002,** *35* (13), 5171-5182.
29. Chevigny, C.; Jestin, J.; Gigmes, D.; Schweins, R.; Di-Cola, E.; Dalmas, F.; Bertin, D.; Boue, F., "Wet-to-Dry" Conformational Transition of Polymer Layers Grafted to Nanoparticles in Nanocomposite. *Macromolecules* **2010,** *43* (11), 4833-4837.
30. Buenning, E.; Jestin, J.; Huang, Y.; Benicewicz, B. C.; Durning, C. J.; Kumar, S. K., Location of Imbibed Solvent in Polymer-Grafted Nanoparticle Membranes. *ACS Macro Letters* **2018,** *7* (9), 1051-1055.
31. Tanaka, H.; Hasegawa, H.; Hashimoto, T., Ordered structure in mixtures of a block copolymer and homopolymers. 1. Solubilization of low-molecular-weight homopolymers. *Macromolecules* **1991,** *24* (1), 240-251.
32. Ojha, S.; Beppler, B.; Dong, H. C.; Matyjaszewski, K.; Garoff, S.; Bockstaller, M. R., Impact of Polymer Graft Characteristics and Evaporation Rate on the Formation of 2-D Nanoparticle Assemblies. *Langmuir* **2010,** *26* (16), 13210-13215.
33. Freeman, B. D., Basis of permeability/selectivity tradeoff relations in polymeric gas separation membranes. *Macromolecules* **1999,** *32* (2), 375-380.
34. Liu, G. P.; Chernikova, V.; Liu, Y.; Zhang, K.; Belmabkhout, Y.; Shekhah, O.; Zhang, C.; Yi, S. L.; Eddaoudi, M.; Koros, W. J., Mixed matrix formulations with MOF molecular sieving for key energy-intensive separations. *Nature Materials* **2018,** *17* (3), 283-+.
35. Rodenas, T.; Luz, I.; Prieto, G.; Seoane, B.; Miro, H.; Corma, A.; Kapteijn, F.; Xamena, F. X. L. I.; Gascon, J., Metal-organic framework nanosheets in polymer composite materials for gas separation. *Nature Materials* **2015,** *14* (1), 48-55.
36. Wang, Y.; Ma, X.; Ghanem, B. S.; Alghunaimi, F.; Pinnau, I.; Han, Y., Polymers of intrinsic microporosity for energy-intensive membrane-based gas separations. *Materials Today Nano* **2018,** *3*, 69-95.

37. Raymond, P. C.; Koros, W. J.; Paul, D. R., COMPARISON OF MIXED AND PURE GAS PERMEATION CHARACTERISTICS FOR CO2 AND CH4 IN COPOLYMERS AND BLENDS CONTAINING METHYL-METHACRYLATE UNITS. *Journal of Membrane Science* **1993,** *77* (1), 49-57.
38. Garnweitner, G.; Goldenberg, L. M.; Sakhno, O. V.; Antonietti, M.; Niederberger, M.; Stumpe, J., Large-scale synthesis of organophilic zirconia nanoparticles and their application in organic-inorganic nanocomposites for efficient volume holography. *Small* **2007,** *3* (9), 1626-1632.
39. Li, C.; Han, J.; Ryu, C. Y.; Benicewicz, B. C., A versatile method to prepare RAFT agent anchored substrates and the preparation of PMMA grafted nanoparticles. *Macromolecules* **2006,** *39* (9), 3175-3183.
40. Bressler, I.; Kohlbrecher, J.; Thunemann, A. F., SASfit: a tool for small-angle scattering data analysis using a library of analytical expressions. *J Appl Crystallogr* **2015,** *48*, 1587-1598.
42. Janes, D. W., Moll, J. F., Harton, S. E., & Durning, C. J.. Dispersion Morphology Of Poly(Methyl Acrylate)/Silica Nanocomposites. *Macromolecules* **2011,** *44*(12), 4920–4927.
43. Bansal, A., Yang, H., Li, C., Cho, K., Benicewicz, B. C., Kumar, S. K., & Schadler, L. S.. Quantitative Equivalence Between Polymer Nanocomposites And Thin Polymer Films. *Nature Materials* **2005**, *4*(9), 693–698.
44. Johannsmann, D., Viscoelastic, Mechanical, And Dielectric Measurements On Complex Samples With The Quartz Crystal Microbalance. *Phys Chem Chem Phys* **2008,** *10* (31), 4516-4534.
45. Jordan, S. M.; Koros, W. J.; Fleming, G. K., The Effects Of Co2 Exposure On Pure And Mixed Gas Permeation Behavior - Comparison Of Glassy Polycarbonate And Silicone-Rubber. *Journal Of Membrane Science* **1987,** *30* (2), 191-212.
46. He, Y.; Benedetti, F. M.; Lin, S. R.; Liu, C.; Zhao, Y. C.; Ye, H. Z.; Van Voorhis, T.; De Angelis, M. G.; Swager, T. M.; Smith, Z. P., Polymers With Side Chain Porosity For Ultrapermeable And Plasticization Resistant Materials For Gas Separations. *Advanced Materials* **2019,** *31* (21).
47. Chiou, J. S.; Barlow, J. W.; Paul, D. R., Plasticization Of Glassy-Polymers By Co2. *J Appl Polym Sci* **1985,** *30* (6), 2633-2642.
48. Genduso, G.; Wang, Y. G.; Ghanem, B. S.; Pinnau, I., Permeation, Sorption, And Diffusion Of Co2-Ch4 Mixtures In Polymers Of Intrinsic Microporosity: The Effect Of Intrachain Rigidity On Plasticization Resistance. *Journal Of Membrane Science* **2019,** *584*, 100-109.
49. Bos, A.; Punt, I. G. M.; Wessling, M.; Strathmann, H., Plasticization-Resistant Glassy Polyimide Membranes For Co2/Co4 Separations. *Sep Purif Technol* **1998,** *14* (1-3), 27-39.
50. Ferry, J. D., *Viscoelastic Properties Of Polymers*. 3d Ed.; Wiley: New York, 1980; P Xxiv, 641 P.
54. Honerkamp, J.; Weese, J., A Nonlinear Regularization Method For The Calculation Of Relaxation Spectra. *Rheol Acta* **1993,** *32* (1), 65-73.
52. De Angelis, M. G.; Merkel, T. C.; Bondar, V. I.; Freeman, B. D.; Doghieri, F.; Sarti, G. C., Gas Sorption And Dilation In Poly(2,2-Bistrifluoromethyl-4,5-Difluoro-1,3-Dioxole-Co-Tetrafluoroethylene): Comparison Of Experimental Data With Predictions Of The Nonequilibrium Lattice Fluid Model. *Macromolecules* **2002,** *35* (4), 1276-1288.
53. Grest, G. S.; Kremer, K., Molecular-Dynamics Simulation For Polymers In The Presence Of A Heat Bath. *Phys Rev A* **1986,** *33* (5), 3628-3631.
54. Anderson, J. A.; Lorenz, C. D.; Travesset, A., General Purpose Molecular Dynamics Simulations Fully Implemented On Graphics Processing Units. *Journal Of Computational Physics* **2008,** *227* (10), 5342-5359.

55. Glaser, J.; Nguyen, T. D.; Anderson, J. A.; Lui, P.; Spiga, F.; Millan, J. A.; Morse, D. C.; Glotzer, S. C., Strong Scaling Of General-Purpose Molecular Dynamics Simulations On Gpus. *Comput Phys Commun* **2015,** *192*, 97-107.
56. Martyna, G. J.; Tuckerman, M. E.; Tobias, D. J.; Klein, M. L., Explicit Reversible Integrators For Extended Systems Dynamics. *Mol Phys* **1996,** *87* (5), 1117-1157.
57. Martyna, G. J.; Tobias, D. J.; Klein, M. L., Constant-Pressure Molecular-Dynamics Algorithms. *J Chem Phys* **1994,** *101* (5), 4177-4189.

Supporting Materials:

Materials and Methods

Figures S1-S28

Tables S1-S7

References (44-57)

Acknowledgments: Financial support for this work was provided by the National Science Foundation Graduate Research Fellowship Program (CRB: grant #DGE-16-44869) and the DMREF Program (CRB, MJ, SKK: grant #1629502). BCB and YH acknowledge support from the SC SmartState program. AN and JM acknowledge funding from the German Research Foundation (DFG) through project NI 1487/2-1. Funding of PLEPS within the BMBF project 05K16WN1-Positec is acknowledged.

Image for Table of Contents: